

Quantum Electrodynamics vacuum polarization solver

P. Carneiro^a, T. Grismayer^a, R. A. Fonseca^{a,b}, L. O. Silva^a

^a*GoLP/Instituto de Plasmas e Fusão Nuclear, Instituto Superior Técnico, Universidade de Lisboa, 1049-001 Lisbon, Portugal*

^b*DCTI/ISCTE - Instituto Universitário de Lisboa, 1649-026 Lisboa, Portugal*

Abstract

The self-consistent modeling of vacuum polarization due to virtual electron-positron fluctuations is of relevance for many near term experiments associated with high intensity radiation sources and represents a milestone in describing scenarios of extreme energy density. We present a generalized finite-difference time-domain solver that can incorporate the modifications to Maxwell's equations due to virtual vacuum polarization. Our multidimensional solver reproduced in one dimensional configurations the results for which an analytic treatment is possible, yielding vacuum harmonic generation and birefringence. The solver has also been tested for two-dimensional scenarios where finite laser beam spot sizes must be taken into account. We employ this solver to explore different types of counter-propagating configurations that can be relevant for future planned experiments aiming to detect quantum vacuum dynamics at ultra-high electromagnetic field intensities.

Keywords:

QED polarization, Maxwell solver, Finite Difference Time Domain

1. Introduction

The prospects offered by ultra-intense laser sources (in the infra-red (IR) or x-ray central wavelengths [1]) have triggered a renewed interest in Quantum Electrodynamics (QED) and its impact on quantum processes at a macroscopic scale, namely how such phenomena can affect well studied interactions in the fields of plasma and laser dynamics. The most relevant QED processes in strong fields and high intensity laser interactions have been explored in several reviews [2, 3]. Among these effects, the second order QED process of photon-photon scattering mediated by the vacuum fluctuation of virtual electron-positron pairs has been a topic of renewed interest motivated by several exotic consequences [3, 4, 5, 6] that originate directly from the original Heisenberg & Euler Lagrangian [7]. However, many of these effects, such as the virtual polarization of the vacuum, remain to be experimentally observed. With expected peak intensities up to $10^{23} - 10^{24}$ Wcm⁻² to be delivered by large scale facilities such as the Extreme Light Infrastructure (ELI) [8], the VULCAN 20 PW project [9], or the HERCULES laser upgrade [10], the regime where these virtual fluctuations

can be detected is close to being within reach. In particular, experiments are being planned to study the quantum dynamics of the vacuum [11] by combining ultra-intense IR lasers with x-ray lasers [12]. The increasing consensus regarding the importance of quantum dynamics in the collective effects of many extreme laser plasma systems has motivated the development of novel numerical tools that couple the multiple scales associated with the problem. Numerical codes that simulate quantum radiation reaction [13, 14, 15] and pair production effects [16, 17, 18, 19, 20], have already made important predictions in extreme energy density scenarios [20, 21, 22]. However, a method to include the effect of vacuum polarization via the creation of virtual pairs, in multi-dimensions and for a broad set of initial conditions, has not been proposed yet. In particular, the ability to fully self-consistently couple the dynamics of relativistic particles with the various ultra-high intensity processes with vacuum polarization effects has not been accomplished. As further shown in this paper, these vacuum quantum effects can be integrated via an effective nonlinear permeability and permittivity that allows us to adopt a semi-classical approach. The effects of the quantum vacuum can be important not only in scenarios involving high intensity electromagnetic radiation but also in the description of the formation and

Email address:

pedro.vidal.carneiro@tecnico.ulisboa.pt (P. Carneiro)

Preprint submitted to Elsevier

July 15, 2016

dynamics of the magnetosphere of pulsars [23].

The electron-positron pair vacuum fluctuations were first taken into account by Heisenberg and Euler (HE) who calculated the first full corrected Lagrangian to all orders. In the low field $E \ll E_s$, low frequency $\omega \ll \omega_c$ limit of the electromagnetic (EM) fields, the leading corrections of the standard Maxwell Lagrangian density [7] can be written as

$$\mathcal{L} = \varepsilon_0 \mathcal{F} + \xi(4\mathcal{F}^2 + 7\mathcal{G}^2), \quad (1)$$

where the Compton frequency is given by $\omega_c = m_e c^2 / \hbar$, the Schwinger critical field $E_s = m_e^2 c^3 / e \hbar$ and the EM invariants $\mathcal{F} = E^2 - c^2 B^2$ and $\mathcal{G} = \vec{E} \cdot \vec{B}$. The nonlinearities coupling parameter is

$$\xi = \frac{20\alpha^2 \varepsilon_0^2 \hbar^3}{45m_e^4 c^5} \sim 10^{-51} [\text{Fm/V}^2]. \quad (2)$$

This parameter weights the relative importance of the quantum corrections compared to the classical fields and vanishes in the limit $\hbar \rightarrow 0$. Calculating the Euler-Lagrange equations for the electromagnetic fields, we obtain a set of modified Maxwell equations [5]

$$\vec{\nabla} \cdot \vec{D} = 0 \quad (3a)$$

$$\vec{\nabla} \cdot \vec{B} = 0 \quad (3b)$$

$$\vec{\nabla} \times \vec{H} - \frac{\partial \vec{D}}{\partial t} = 0 \quad (3c)$$

$$\frac{\partial \vec{B}}{\partial t} + \vec{\nabla} \times \vec{E} = 0, \quad (3d)$$

with

$$\vec{D} = \varepsilon_0 \vec{E} + \vec{P} \quad (4a)$$

$$\vec{B} = \mu_0 \vec{H} + \vec{M}. \quad (4b)$$

In this approach, the effect of the quantum dynamics, arising from vacuum fluctuations modifies Ampère's law by a nonlinear vacuum polarization, \vec{P} , and magnetization, \vec{M} , given by

$$\vec{P} = 2\xi [2(E^2 - c^2 B^2)\vec{E} + 7c^2(\vec{E} \cdot \vec{B})\vec{B}] \quad (5)$$

$$\vec{M} = -2\xi [c^2(2(E^2 - c^2 B^2)\vec{B} - 7(\vec{E} \cdot \vec{B})\vec{E})]. \quad (6)$$

This semi-classical formulation effectively treats the vacuum as a nonlinear medium, being relevant when the EM invariants are non zero. In this paper, we present an algorithm to solve the nonlinear set of corrected Maxwell's equations in a self-consistent manner. This algorithm is second order accurate in time and in space.

Due to its design, a key feature of the algorithm is that it can be incorporated into massively parallel fully relativistic electromagnetic particle-in-cell codes such as OSIRIS [24].

This paper is organized as follows. In section 2, we describe the numerical algorithm, a generalization of the Yee algorithm, that solves eqs.(3a-5) in multi-dimensions. The one-dimensional results are presented in section 3, including a detailed comparison between the simulations and analytical models for several physical mechanisms including vacuum birefringence. In section 4, multi-dimensional results are displayed as an illustration of the method, with an emphasis on harmonic generation and finite beam effects. Finally in section 5 we state the conclusions.

2. Numerical Algorithm

In this section we first provide a description of the algorithm, followed by a detailed discussion of the important aspects of the field interpolation. The stability of the algorithm is also considered.

2.1. Description

A standard finite-difference time domain (FDTD) method to solve Maxwell's equations is the Yee Algorithm [25]. The Yee scheme solves simultaneously for both electric and magnetic fields by solving Faraday's and Ampère's law, respectively. The explicit linear dependence of Maxwell's equations on the fields allows the field solver to be centered both in space and time (leap frog scheme), thus providing a robust, second order accurate scheme without the need to solve for simultaneous equations or matrix inversion [26]. Moreover, the efficiency and simplicity of the Yee scheme allow an easy incorporation into numerically parallel PIC codes.

To solve the QED Maxwell equations, a modified Yee scheme was developed to address the two main difficulties which arise from the nonlinear terms. Firstly, all fields must be evaluated at all grid positions as opposed to spatially staggered fields. This permits to accurately evaluate quantities such as the EM invariants \mathcal{F} and \mathcal{G} , since a given component of the nonlinear polarization and magnetization vectors now fully couples all other field components as can be understood from eqs.(5-6). This is a significant obstacle regarding the essence of the Yee scheme since the algorithm may no longer be correctly spatially centered. Secondly, the temporal derivative of the nonlinear polarization term in Ampère's equations prevents each electric field component to be advanced in a straightforward manner as it

requires the knowledge of future quantities. This is easily understood through the discretization of the modified Ampère's law in one dimension

$$-\frac{1}{\mu_0} \frac{B_{z,i+1/2}^{n+1/2} - B_{z,i-1/2}^{n+1/2}}{\Delta x} + \frac{M_{z,i+1/2}^{n+1/2} - M_{z,i-1/2}^{n+1/2}}{\Delta x} = \epsilon_0 \frac{E_{y,i}^{n+1} - E_{y,i}^n}{\Delta t} + \frac{P_{y,i}^{n+1} - P_{y,i}^n}{\Delta t}, \quad (7)$$

where the indices n and i denote the temporal and spatial positions, respectively. Usually, one would isolate the electric field term of temporal index $n + 1$ to advance this field in time. However, to calculate this component one must know the polarization at time step $n + 1$, which is a nonlinear function of all other fields at the new time step. The latter difficulty served as the main motivation to develop the modified Yee scheme proposed here. The scheme is illustrated in Fig.1 for a time step Δt :

- we begin by advancing the fields using the standard Yee scheme (i.e. without accounting for the polarization and magnetization of the vacuum). This setup allows us to obtain predicted quantities for the values of the fields at the new time. This approach is based on the standard technique of the predictor-corrector method, where the linear Maxwell equations are solved as the zeroth order solution to the fields;
- the predicted field values are then interpolated at all spatial grid points using a cubic spline interpolation method thus allowing to calculate quantities such as the EM invariants and respective polarization and magnetization of the vacuum, to lowest order;
- the polarization and magnetization are then used to advance the electric field via the modified Ampère's law;
- the convergence loop re-injects this new electric field value back into the polarization and magnetization source terms to refine these quantities and re-calculate the electric field iteratively. This loop is reiterated until the electric converges to a value within the desired accuracy;
- after convergence is achieved, Faraday's law is advanced, identically to the linear Yee scheme, benefiting from the fact that the electric field values being used are self-consistent with the QED corrections.

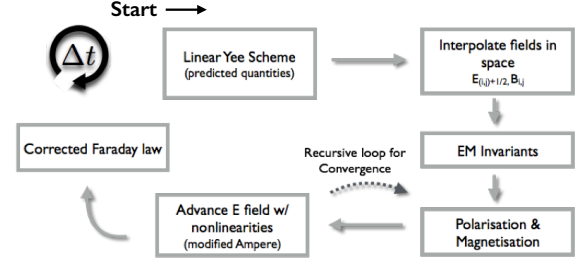


Figure 1: Full loop of the modified Yee scheme

It must be emphasized that this method is only valid as long as the effects of the polarization and magnetization of the medium are small compared to the non-perturbed propagation of the fields given as solutions to Maxwell's equations in classical vacuum. This condition is automatically satisfied for realistic values of electromagnetic fields available in current, or near future, technology. In this regime, the QED theory is valid since the Schwinger field, above which the production of real electron-positron pairs is possible, corresponds to an electric field of $E_s \sim 10^{18}$ V/m, whereas ambitious laser facilities aim to push available intensities to the $10^{23} - 10^{24}$ W/cm² ($E \sim 10^{15}$ V/m) range. The order of the ξ parameter in eqs.(2,5,6) clearly helps to ensure the validity of the method. Therefore, this scheme highly benefits from the fact that the nonlinear QED corrections of the vacuum are perturbative in nature. The convergence loop can be seen as a Born-like series since for every re-insertion of the fields back into the nonlinear source term, there is a gain in accuracy of one order in the expansion parameter to the result. The algorithm proposed here solves Ampère's law by treating the nonlinear corrections as a source term, in an iterative manner,

$$\vec{\nabla} \times \vec{B} - \partial_t \vec{E} = \vec{S}_{NL}[E, B], \quad (8)$$

where $\vec{S}_{NL} = \vec{\nabla} \times \vec{M} + \partial_t \vec{P}$. From this discussion and eq.(8), we can conclude that this generalization of the Yee scheme can be extended beyond the framework of QED corrections to the vacuum as it is valid to solve Maxwell's equations in any nonlinear medium provided that the polarization and magnetization are given and that their order is such that they can be treated as a perturbation. This possible generalization enhances the range of applicability of our algorithm. Furthermore, the inclusion of a current in the algorithm ($J \neq 0$ in Ampère's law) can be done, both within a PIC framework or for a macroscopic field dependent current by including the current term in the initial standard Yee scheme loop where the predictor quantities are com-

puted. This is another key feature regarding the ability to couple our proposed generalized Yee solver to the PIC framework.

2.2. Interpolation of the fields

The algorithm requires that all fields are calculated at the same spatial positions. When considering the spatial interpolation of the self-consistent fields given by the Yee Algorithm we found a clear asymmetry between interpolating the electric field at the magnetic field position or vice-versa in terms of the precision of the EM invariant $E^2 - B^2$ for both cases. Since a plane wave is a trivial solution of the QED Maxwell equations, the invariants calculated in the simulation should be identically zero [27]. Figure 2 shows the distribution of the EM fields within a two-dimensional Yee grid cell. We found that all the standard interpolation schemes yield invariants with much greater precision at the lower left corner of the cell compared to the other positions. This difference in precision was found to be of two orders of magnitude when tested for a plane wave in 1D, which can affect the stability and precision of the code. The reason for this artifact is due to the way that the fields are initialized within the simulation domain. In particular, the fact that the electric and magnetic fields must be initialized with a shift both in space and time, creates an asymmetry between interpolating a field to the corresponding position of the other field, even if this interpolation is done in a centered manner. The solution we have adopted to address this problem is to calculate all the fields at the cell corner where the invariants are known to be of higher precision. For instance, the B_z component at the left corner of the cell becomes

$$B_{z\ i,j} = \mathcal{I}(B_{z\ i+\frac{1}{2},j+\frac{1}{2}}, B_{z\ i-\frac{1}{2},j+\frac{1}{2}}, B_{z\ i+\frac{1}{2},j-\frac{1}{2}}, B_{z\ i-\frac{1}{2},j-\frac{1}{2}}),$$

where \mathcal{I} is an interpolation function. Once all fields are calculated at the (i, j) positions, we can compute the invariants at these positions and then re-interpolate these invariants directly to the other grid cell points in a similar fashion. The correct calculation of the EM invariants is necessary in order to evaluate the nonlinear polarization and magnetization of the vacuum via eqs.(5,6)

2.3. Numerical Stability

The method adopted to study the numerical stability of the QED polarization solver follows the standard mode analysis [26]. With the linear Yee scheme, the one-dimensional numerical dispersion relation for a

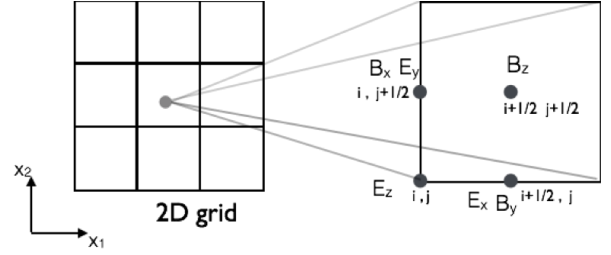


Figure 2: Position of the electric and magnetic field vector components within a 2D cell of the Yee lattice.

plane wave propagating on a grid with spatial and temporal resolution Δx and Δt respectively is [26]

$$\omega_0 = \frac{1}{\Delta t} \arccos \left(1 + \left(\frac{c\Delta t}{\Delta x} \right)^2 (\cos(k\Delta x) - 1) \right). \quad (9)$$

A notable case is when $\Delta t = \Delta x/c$ for which eq.(9) reduces to the EM dispersion relation for a plane wave in vacuum, $\omega_0 = ck$. To study the stability of the new set of QED-corrected Maxwell's equations using this method, a self-consistent numerical dispersion relation was derived. Due to the non-linearity of the equations, the new dispersion relation can be written as

$$\left(\frac{c\Delta t}{\Delta x} \right)^2 \sin^2 \left(\frac{k\Delta x}{2} \right) - \sin^2 \left(\frac{\omega\Delta t}{2} \right) = \xi E_0^2 F_{NL}(\omega, k, \Delta x, \Delta t), \quad (10)$$

where E_0 is the amplitude of the wave and F_{NL} is a nonlinear function of ω , k , and the spatial and temporal steps. In the classical limit $\xi \rightarrow 0$ the RHS goes to zero and the dispersion relation reduces to eq.(9). A numerical plane wave propagating via our QED solver will therefore obey eq.(10).

For a numerical plane wave the EM invariant $\vec{E} \cdot \vec{B}$ is identically zero, whereas the invariant $E^2 - B^2$ will not vanish identically due to finite spatial resolution and the fact that the fields must be interpolated in space to evaluate the invariants, as already discussed above. Therefore, the amplitude of this EM invariant depends on the interpolation method and grid resolution. We calculate this dependence by evaluating $E^2 - B^2$ at a given grid point, taking into account that a correct centering in space implies one of the fields must be interpolated to the position of the other (in this case the B field, using linear interpolation). This yields

$$\text{Inv}(k, \omega) = E_0^2 \left[1 - \frac{\sin^2(k\Delta x/2)}{\sin^2(\omega\Delta t/2)} \cos^2 \left(\frac{k\Delta x}{2} \right) \right]. \quad (11)$$

Where $\text{Inv}(k, \omega)$ represents the Fourier amplitude defined by $\text{Inv}(k, \omega) = (E^2 - B^2)(k, \omega)$ This expression was

compared to the results extracted from one-dimensional simulations. Figure 3 shows a comparison between eq.(11) and simulations with several seeded k modes and with $\xi E_0^2 = 10^{-4}$, $\Delta t = 0.98\Delta x$ and $\Delta x = \pi/100$. The simulation points agree with the trend presented by

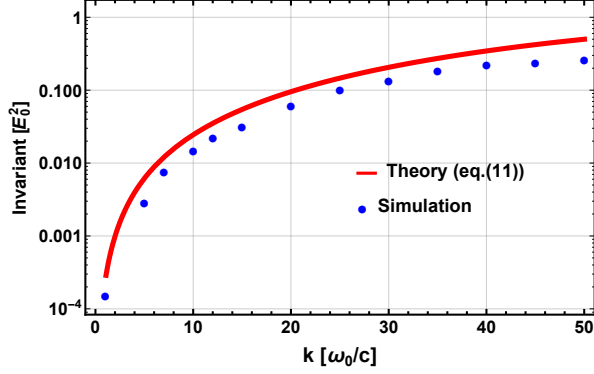


Figure 3: Amplitude of EM invariant $E^2 - B^2$ as a function of the seeded k -mode for a resolution $\Delta x = \pi/100$, $\Delta t = 0.98\Delta x$ and $\xi E_0^2 = 10^{-4}$. Simulation results in blue are compared to eq.11 in red.

the theoretical curve. This result shows that eq.(11) provides an upper bound to the interpolation error when seeding a particular k mode. In particular, the results show that for higher wave numbers, up to the resolution limit, the order of magnitude of the invariant amplitude increases, tending towards unity. One shall therefore limit the simulations to low k modes in order to insure the smallness of the invariants.

The stability of the QED Yee solver, i.e., the nonlinear dispersion relation, eq.(10) was solved using three methods: a numerical solution, an analytical solution through the linearization of the system via the ansatz $\omega = \omega_0 + \delta\omega$ with $\delta\omega \ll \omega_0$, and finally by estimating the growth rate of the maximum mode allowed by the grid resolution i.e. $k\Delta x = \pi$. The results are shown in Fig. 4 for simulations performed with a grid resolution of $\Delta x = 0.0314$, $\Delta t = 0.98\Delta x$ and $\xi E_0^2 = 10^{-4}$. One can verify in Fig.4 that the analytic solution is in excellent agreement with the numerical integration. The maximum growth rate is given by

$$\text{Im}(\delta\omega_{\max}) \simeq \frac{2\xi E_0^2 \sqrt{8\varepsilon}}{\Delta t}, \quad (12)$$

where $\varepsilon = 1 - \frac{\Delta t}{\Delta x}$. The maximum growth rate predicted theoretically serves therefore as an accurate rule-of-thumb criteria to understand how unstable a given simulation setup may be. Finally we took the solution of the perturbative expansion and studied the limit for

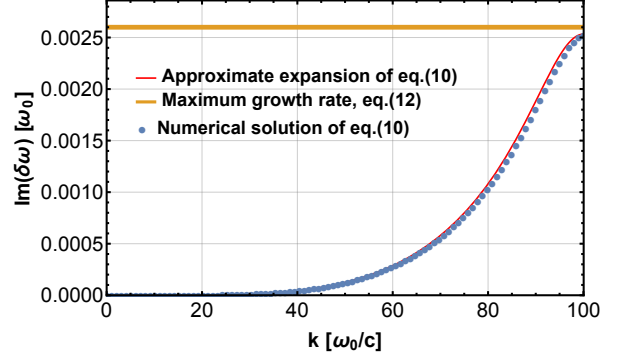


Figure 4: Imaginary part of solution of nonlinear dispersion relation, eq.(10), as a function of k -mode, calculated using three different methods. Simulation parameters used were $\Delta x = 0.0314$, $\Delta t = 0.98\Delta x$ and $\xi E_0^2 = 10^{-4}$.

small k values, which yields

$$\lim_{k\Delta x \rightarrow 0} \text{Im}(\delta\omega) = \frac{1}{4} \frac{\xi E_0^2 (k\Delta x)^5}{\Delta x}. \quad (13)$$

Eq.(13) suggests that the smallest k modes will be the ultimately stable as not only does the growth rate scale with the small quantity ξE_0^2 , but also due to the power law applied to the small value of $k\Delta x$. This is an important result since, in principle, the low k modes, for a given grid resolution, are those that will be seeded for a simulation setup.

These theoretical predictions were compared with one-dimensional simulations by extracting the growth rate of a given k mode in the simulation domain, the results are shown in Fig.5. The growth rate was extracted from the Fourier spectrum of the simulations for different values of ξE_0^2 . Figure 5 shows a close agreement between the maximum growth rates extracted and eq.(12). Our theoretical analysis shows that the growth rate of the most unstable mode scales linearly with ξE_0^2 . Furthermore, we performed simulations under the same conditions, varying only the seeded k mode and verified that this does not affect the growth rate of the most unstable high k modes. Instead, it is the amplitude of the seeded mode that affects the growth rate of the higher k modes by nonlinear coupling. It is possible to derive a criteria for the time at which the seeded field starts to be strongly deteriorated by the growing numerical noise, by assuming this blow-up occurs once the amplitude of the fastest growing k -modes $\delta\tilde{E}$ (initially this amplitude is at the numerical noise level, and can be measured from the initial spectrum of the fields in the simulation), become of the order of the initial seed amplitude. This

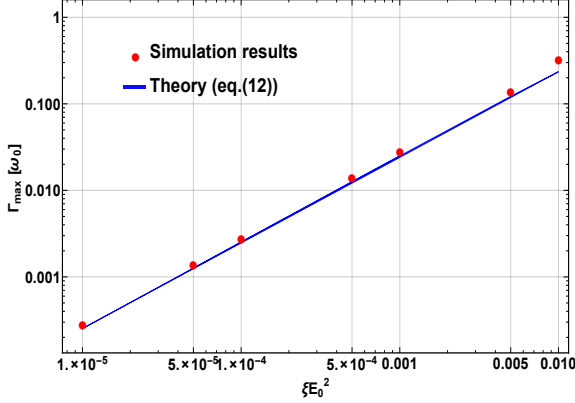


Figure 5: Comparison between maximum growth rate extracted from simulation with theoretical prediction calculated from the nonlinear dispersion relation. The Figure shows how this growth rate varies as a function of ξE_0^2 , which measures the importance of the nonlinear quantum vacuum corrections. The simulation parameters used were $\Delta x = 0.0314$, $\Delta t = 0.98\Delta x$ and a seeded $k_{\text{seed}} = 1$.

criteria yields,

$$t_{\text{blow}} \sim \frac{\Delta t}{\sqrt{\epsilon}} \frac{1}{\xi E_0^2} \log\left(\frac{E_0}{\delta \tilde{E}}\right). \quad (14)$$

For realistic values of ξE_0^2 , this time is far greater than any simulation setup one may wish to perform.

3. 1D Results

A thorough benchmark of the functionality and robustness of the algorithm may only be gained by comparing simulation results with analytical results in 1D simplified cases. One dimensional scenarios provide excellent opportunities to test the code against analytical predictions. The two cases we exploit here are the vacuum birefringence in the presence of a strong static field and counter propagating plane waves. Whilst the first case is well studied in the literature [28, 29], the second case requires a finer analytical work, yielding nevertheless the well known result of generation of higher harmonics due to the nonlinear interaction as shown in [30, 31, 32] in different setups and physical regimes. The true physical value of the parameter in normalized units of the simulation is $\xi \sim 1 \times 10^{-15}$. Simulations were performed with increased values of the ξ parameter in order to better illustrate the method proposed here. This does not alter the physical relevance of the results. Rather, this is simply a re-scaling of a constant in order to highlight the effects in a clearer way. Finally, in all the results presented in this section, the units

were normalized to the characteristic laser frequency, ω_0 and wave number, k_0 . The normalizations are thus $t \rightarrow \omega_0 t$ and $x \rightarrow k_0 x$. These normalizations of space and time define the normalizations used for the fields, i.e: $E \rightarrow eE/mc\omega_0$ and $B \rightarrow eB/mc\omega_0$.

3.1. Vacuum Birefringence

The birefringence of the vacuum is a thoroughly studied setup of great experimental interest to explore the properties of the quantum vacuum [33]. A one dimensional wave packet traveling in the presence of a strong static field will experience a modified refractive index of the vacuum due to the HE corrections. To obtain an approximate analytical expression, one assumes that the strong background field remains unperturbed by the nonlinearities. This motivates the following ansatz for the solution of modified Maxwell's equations

$$\vec{E} = \vec{E}_p(x, t) + \vec{E}_s, \quad (15)$$

where E_p and E_s represent the electromagnetic pulse and the static fields, respectively and $E_p \ll E_s$. Inserting eq.(15) into the QED Maxwell's equations and keeping only the dominant terms in the polarization and magnetization, one obtains the following refractive indexes:

$$n_{\parallel} = \left(\frac{1 + 6\xi E_s^2}{1 + 2\xi E_s^2} \right)^{1/2}, \quad (16)$$

$$n_{\perp} = \left(\frac{1 + 2\xi E_s^2}{1 - 5\xi E_s^2} \right)^{1/2}, \quad (17)$$

where the parallel and perpendicular directions refer to the direction of the probe polarization when compared to the static field. Notice that the product ξE_s^2 appears as a relevant quantity. This is a recurring property of several setups. It must be ensured that this product is a small quantity, both for the validity of the theoretical framework but also from the algorithm point of view. This quantity controls whether the corrections to the unperturbed fields are small or not, a crucial feature for the stability of algorithm as, already discussed.

The simulation setup consists of a strong static electric field of $10^{-3} E_s$ aligned along the y direction and a Gaussian EM pulse propagating in the x direction and polarized in the $y - z$ plane. The central wavelength of the EM Gaussian pulse is $1 \mu\text{m}$ and its duration 5.6 fs. Figure 6 shows two simulations for the same pulse after propagating once through a periodic box. In one case the propagation is in the classical vacuum, whereas the QED solver is used in the other. Qualitatively, the difference in propagation distance and the reduced electric field amplitude is consistent with the theory of a

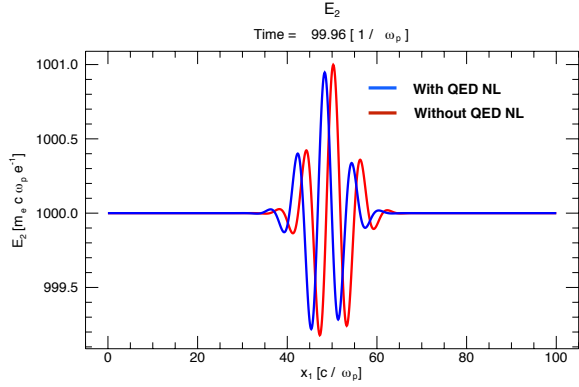


Figure 6: 1D Gaussian pulse after an entire propagation over a periodic box in the presence of a strong static field, with (blue) and without (red) QED nonlinearities

pulse traveling in a refractive medium. To test the accuracy of the algorithm this same setup was run for different values of the product ξE_s^2 for both the parallel and perpendicular setup. The difference in phase velocity between the two pulses allows to extract directly the quantum vacuum refractive indexes and to compare with the analytical predictions of eq.(16)-eq.(17). The results are shown in Fig. 7(a) and Fig.7(b) where an excellent agreement between simulation and theory is found. This 1D setup is useful, since the strong static field could model the electric field of another pulse with a much smaller frequency (static approximation).

3.2. Counter-propagating plane waves

Considering a 1D periodic box with two counter-propagating plane waves polarized in the y direction, with the same frequency and amplitude, we can test how this interaction, which would normally result in a standing wave, is modified in the presence of the HE nonlinearities. This example also serves as an ideal benchmark for the accuracy and stability of the code, provided an exact analytic result can be obtained.

The theoretical analysis to address this scenario is similar to a Born series of partial waves. Assuming that the solution of the QED Maxwell's equations are of the type

$$E = E_{(0)} + E_{(1)} + E_{(2)} + \dots \quad (18)$$

$$B = B_{(0)} + B_{(1)} + B_{(2)} + \dots, \quad (19)$$

where $E_{(0)}$ and $B_{(0)}$ are the unperturbed standing wave fields given by $E_{(0)} = E_0 [\cos(x-t) + \cos(x+t)]$ and $B_{(0)} = B_0 [\cos(x+t) - \cos(x-t)]$ whilst the remaining terms are successively higher order corrections to

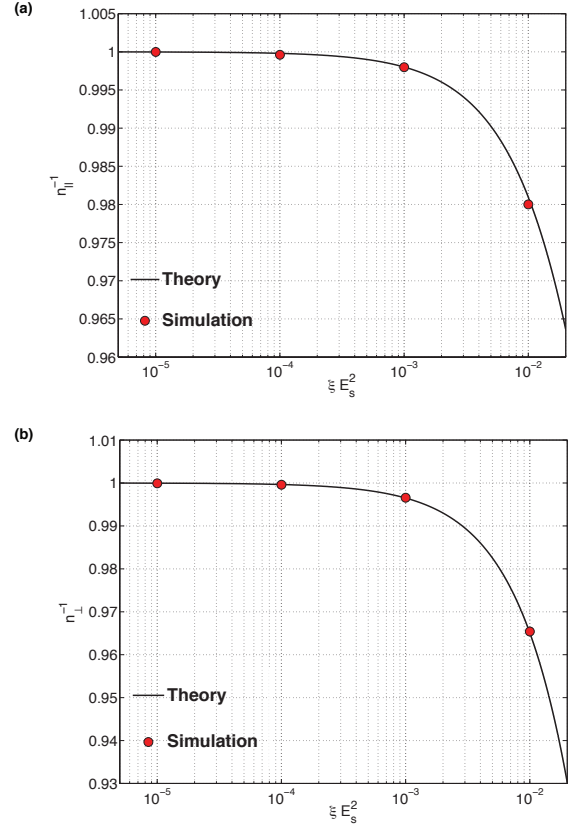


Figure 7: (a) Phase velocity ($c = 1$) of probe pulse with polarization parallel to E_s , (b) Phase velocity ($c = 1$) of probe pulse with polarization perpendicular to E_s , both as a function of ξE_s^2 parameter

the standing wave fields, weighted by an expansion parameter to be identified. Starting from the modified Maxwell's equations and inserting eq.(18) and eq.(19) as the expressions for the fields, we arrive at the wave equation for the first order correction to the electric field $E_{(1)}$

$$\square E_1 = S_1(x, t), \quad (20)$$

where \square is the d'Alembert operator and the source term $S_1 = -\partial_t \partial_x M + \partial_t^2 P$. Inserting in the source term, the zero order field, i.e. $P, M = f(E_{(0)}, B_{(0)})$, we arrive at

$$S_{(1)}(x, t) = 16\xi E_0^3 \cos(t) \cos(x) [3 \cos(2t) - \cos(2x)] \quad (21)$$

This source term only accounts for the unperturbed fields being inserted into the nonlinear polarization and magnetization. The formal solution of this equation is given by the convolution between the source term and the Green's function of the one dimensional wave oper-

ator [34],

$$E_{(1)}(x, t) = \int_0^L \int_0^t dt' dx' G(x, x', t, t') S(x', t') \quad (22)$$

where the Green's function is

$$G(x, x', t, t') = \frac{1}{2} H((t - t') - |x - x'|) \quad (23)$$

The modified electric field reads

$$E_{(1)}(x, t) = -2\xi E_0^3 \sin(t) \cos(x) [2 \sin(2t) (\cos(2x) - 2) - 4t]. \quad (24)$$

The corrected field exhibits a secular growth term modulated by an oscillating term. We also notice that the relative amplitude between this term and the unperturbed field amplitude is ξE_0^2 showing again that this perturbative treatment is valid as long as $\xi E_0^2 \ll 1$. Taking the spatial Fourier transform of $E_{(1)}$, we verify that the fundamental mode $k = k_0$ is reinforced by the linearly growing term and the appearance of an harmonic at $k = 3k_0$. Defining the Fourier transform of $E(x, t)$ as $\tilde{E}(k, t)$, we obtain

$$\tilde{E}_{(1)}(k = k_0) = 4\xi E_0^3 t \sin(t) + 3\xi E_0^3 \sin(t) \sin(2t), \quad (25)$$

$$\tilde{E}_{(1)}(k = 3k_0) = -\xi E_0^3 \sin(t) \sin(2t). \quad (26)$$

The next order correction to the field $E_{(2)}$, reveals a $k = k_0$ harmonic growing as t^2 , a secular $k_0 = 3k_0$ term and an oscillating $k = 5k_0$ term. Repeating this process to higher orders, we can show that this nonlinear interaction generates odd higher harmonics from vacuum with the relative amplitude between these harmonics obeying the ordering

$$\tilde{E}(k = 2n + 1) = (\xi E_0^2)^n \tilde{E}(k = k_0) \quad (27)$$

These predictions were compared with the results of the QED solver using field amplitude of $E_0 = 0.025E_s$, $\lambda_0 = 1 \mu\text{m}$ plane waves and $\xi = 10^{-9}$, such that the higher harmonics can be accurately resolved above the numerical noise. The spatial Fourier transform of the fields at a certain time is shown in Fig. 8 for two simulations, with and without the self-consistent inclusion of HE corrections. We observe that when the nonlinearities are present, the odd higher harmonics are generated with a relative amplitude that matches the ordering given in eq.(27). In order to compare the simulation results with eqs.(25,26), we subtracted the classical vacuum electric field to remove the zeroth order standing wave contribution, and performed the Fourier transform of this subtracted field. Finally, we tracked the temporal evolution of the amplitude of the $k = k_0$ mode in Fourier

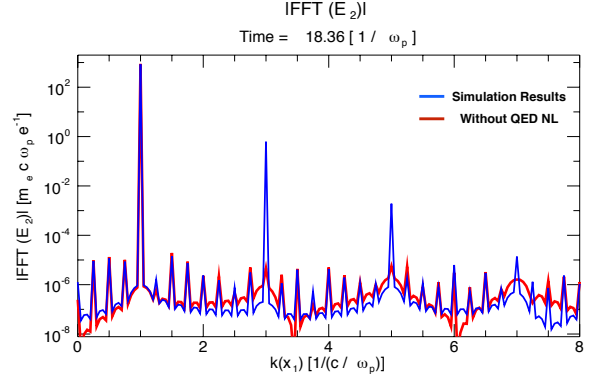


Figure 8: Spatial Fourier transform of electric field with and without QED NL present. The generation of odd higher harmonics can be observed in blue.

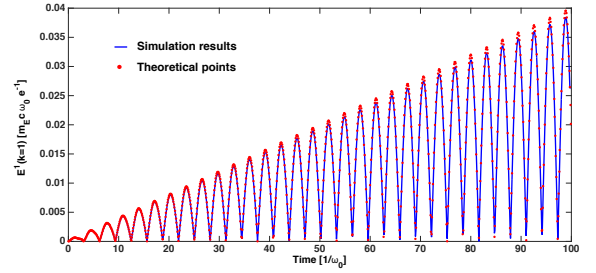


Figure 9: Temporal evolution of $k = k_0$ Fourier mode of the subtracted electric field

space and compared it with eq.(25). Figure 9 shows the temporal evolution of $E_1(k = k_0)$. The simulation shows an excellent agreement with the theoretical predictions for many laser cycles, ensuring that the algorithm is robust. Despite the one dimensionality of this example, a setup of counter-propagating beams is of great interest for planned experiments at extreme high intensity laser facilities, as outlined in [35].

4. 2D Results

In order to illustrate this algorithm in multi-dimensions, two setups were investigated in 2D: the counter propagation of two Gaussian pulses interacting at the focal point, and the perpendicular interaction of two Gaussian pulses focused at the same point. For these setups, a consistent analytical treatment becomes cumbersome especially due to the self-consistent treatment of both the transverse and longitudinal component of the pulses. A quantum parameter of $\xi = 10^{-6}$ was

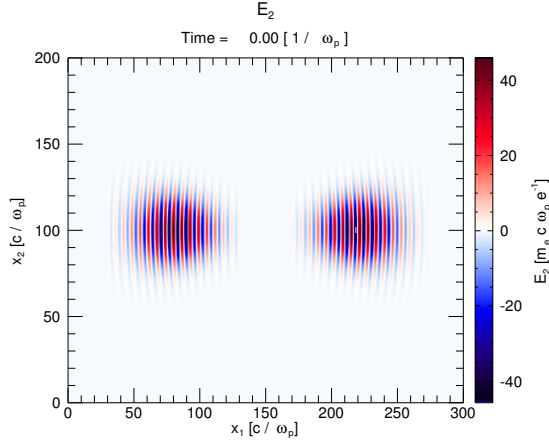


Figure 10: Initial setup of Gaussian pulses. Both pulses are polarized in the x_2 direction and will focus in the center of the box.

used for the sake of providing illustrative examples. In the first setup two $\lambda = 1\mu\text{m}$ laser beams with a normalized vector potential $a_0 = 50$ ($\sim 10^{-4}E_s$ in normalized units) and duration of 25 femtoseconds were counter-propagated and interacted in the presence of the QED nonlinearities. Both beams had a waist $W_0 = 2.3\mu\text{m}$. Figure 10 shows the transverse electric field of the laser beams before interaction, Fig.11-(a) the spatial Fourier transform of the beams with $\xi = 0$ (classical limit) and in Fig. 11-(b) the Fourier transform of the electric field after the interaction (asymptotic state) including the HE corrections. As shown in Fig. 11-(b), after the interaction odd higher harmonics are also generated as in the 1D case, with relative amplitudes consistent with eq.(27). However, in this case the harmonics generated have the same Gaussian behavior as the unperturbed pulses and attain a greater spread in Fourier space after the interaction. After the pulses have spatially overlapped, the harmonics propagate and leave an imprint of the nonlinear interaction, that co-propagates with the original beam.

The second setup shown in Fig. 12 is more rich: it comprises of two $1\mu\text{m}$ Gaussian pulses with $a_0 = 50$ and interact at their focus, with $k_1 \perp k_2$. The beam parameters are equal to those of the previous setup. The initial Fourier space of the beam propagating in the x direction is shown in Fig. 13-(a) and this spectrum would remain unaltered during the interaction in the classical limit ($\xi=0$). During the peak of the nonlinear interaction (at the focal point) we see in Fig. 13-(b) that many pairs of (k_1, k_2) harmonic combinations are being generated. More interestingly, there appears to be a continu-

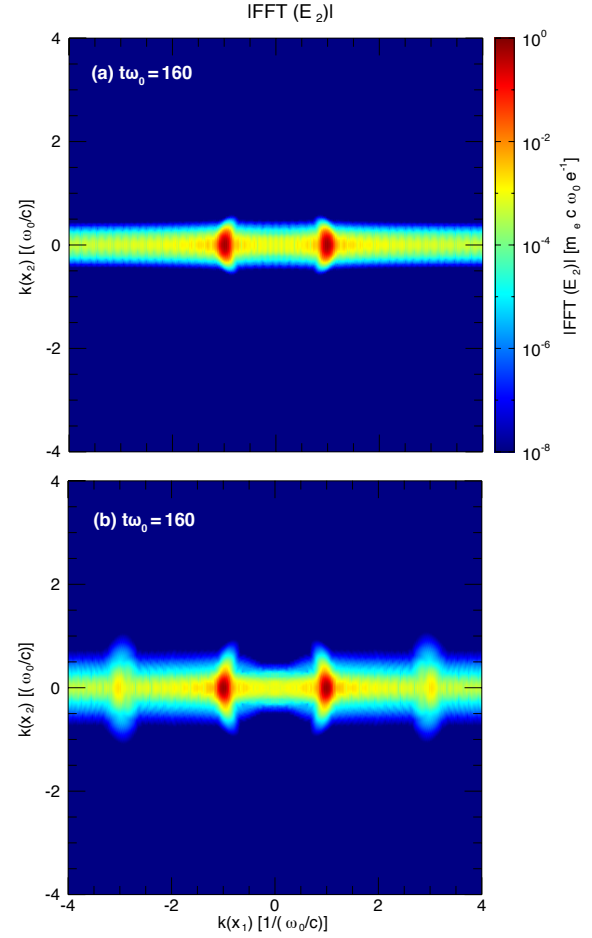


Figure 11: Spatial Fourier transform of the electric field, (a) after the interaction but when QED corrections are absent, (b) after the interaction with self-consistent inclusion of the quantum corrections. $k = 3k_0$ harmonics and small distortion of $k = k_0$ can be observed.

ous filling of Fourier space in between the expected harmonics integer combination as the spatial overlap creates a multitude of nonlinear Gaussian modes. This effect is then lessened after the interaction has occurred since there is no longer a source to feed these regions of Fourier space and only the integer expected combination of (k_1, k_2) harmonics are left as an imprint of the interaction, see Fig. 13-(c). The longitudinal field component triggers a self-interaction of the Gaussian pulse through the QED nonlinearities. This self-interaction plays the role of a coupling source when both pulses interact spatially. Such terms are responsible for the $(k_0, 2k_0)$ and $(2k_0, 2k_0)$ harmonic points in Fig. 13-(b). The self-interaction coupling combined with the different propagation directions, is the reason why this second setup generates several new harmonic couplings, com-

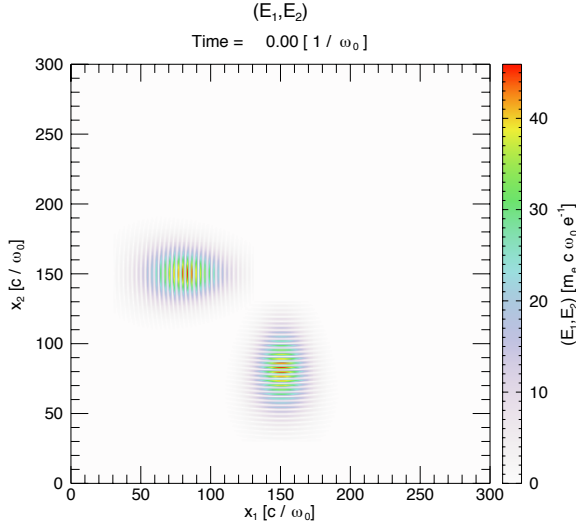


Figure 12: Electric field setup for two Gaussian pulsed traveling in perpendicular directions but focusing on the same point.

pared with the previous counter-propagating setup.

The Fourier spectra obtained in these two setups show that the harmonics generated in either case are distinct, thus allowing to clearly distinguish both cases. Future work will include the analytical study of the relative intensity and spectral width of the generated harmonics and their possible relation with other beam parameters and with the fundamental interaction parameter ξ . Namely, it is of great interest to understand how the production of these higher harmonics from vacuum may be optimized in terms of the duration of the pulses as these results can provide signatures of experimental relevance. A future setup to explore will also include the interaction of two laser beams at an arbitrary angle $0 < \theta < \frac{\pi}{2}$ radians in order to model realistic experimental conditions. If this angular dependence of the interaction is well understood, one could in principle determine how well aligned two ultra-intense beams are by looking at the Fourier spectrum after a vacuum interaction. Finally, if one assumes that the parameter ξ is a well measured quantity, one could precisely measure the initial intensity of the beams. This final property enhances the interest in this analysis in a time where ultra-intense laser facilities are being upgraded or constructed around the world and the experimental techniques to measure such intensities is still not firmly established.

5. Conclusions

A numerically stable and robust generalized Yee scheme to solve the nonlinear set of QED Maxwell's

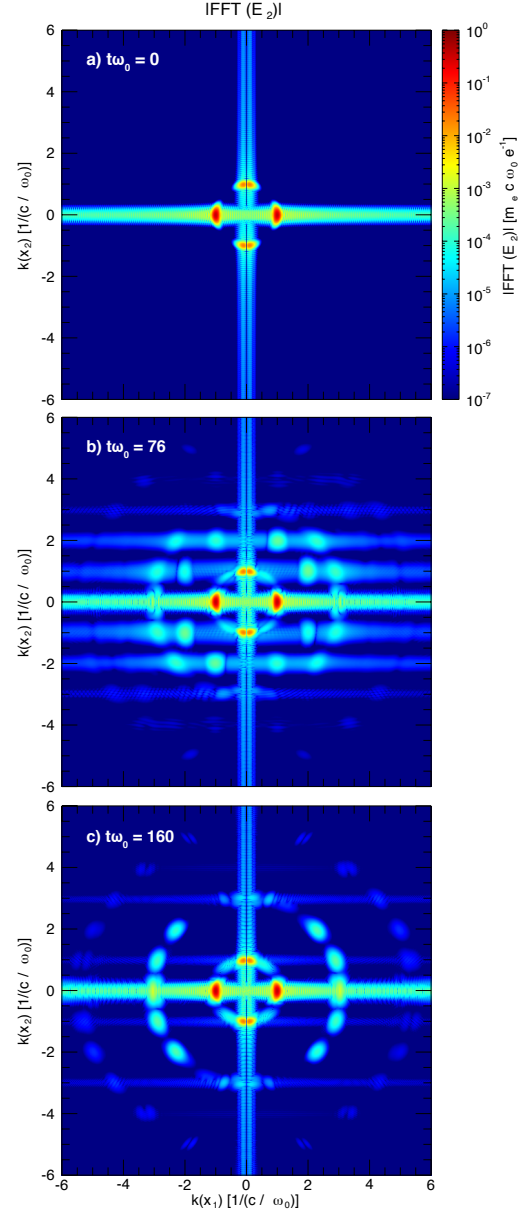


Figure 13: Spatial Fourier transform for E_2 field at different stages of interaction. (a) Initial Fourier space, if there were no vacuum nonlinearities this spectrum would remain unchanged throughout the interaction. (b) At peak of nonlinear interaction when the pulses are completely overlapped in space. (c) Asymptotic state: after the nonlinear interaction the pulses propagate independently but with higher harmonics generated from the interaction.

equations was developed and incorporated in a standard PIC loop. This work represents an important step towards modeling plasma dynamics in extreme scenarios when QED processes significantly alter the collective behavior of the system. Our code can be used to bench-

mark planned experiments, leveraging on ultra-intense laser facilities able to deliver intensities of $10^{23} - 10^{24}$ W/cm², to verify for the first time the dynamics of the quantum vacuum below the Schwinger limit. The simulations confirm predicted optical phenomena such as vacuum birefringence and high harmonics generation in one-dimensional setups with an excellent accuracy. The code was also extended for two-dimensional scenarios where two setups of interacting Gaussian beams were studied. The results highlight the importance of transverse beam effects and hint that the generation of higher harmonics from quantum vacuum can be achieved via this interaction. The spectrum of the harmonics could provide a direct measurement of important beam properties such as the peak intensity and alignment. This algorithm may also be used to test two and three dimensional setups that have been proposed in the literature (where transverse and finite spot size effects are taken into account under certain approximations), thus complementing the results of previous theoretical works [35, 36]. Finally our algorithm contributes to the generalization of the Yee scheme, one of the most successful and commonly used algorithms in computational physics, to scenarios where nonlinear polarization and magnetization can impact EM propagation.

6. Acknowledgements

The authors would like to thank Marija Vranic for a careful revision of the manuscript. This work was supported by the European Research Council (Accelerates ERC-2010- AdG 267841 and InPairs ERC-2015-AdG 695008). Simulations were performed at the ACCELERATES cluster (Lisbon, Portugal).

References

- [1] C. Danson, D. Hillier, N. Hopps, D. Neely, Petawatt class lasers worldwide, *High Power Laser Science and Engineering* 3 (2015) e3.
- [2] A. Di Piazza, C. Müller, K. Z. Hatsagortsyan, C. H. Keitel, Extremely high-intensity laser interactions with fundamental quantum systems, *Rev. Mod. Phys.* 84 (2012) 1177–1228.
- [3] M. Marklund, P. K. Shukla, Nonlinear collective effects in photon-photon and photon-plasma interactions, *Rev. Mod. Phys.* 78 (2006) 591–640.
- [4] G. V. Dunne, The heisenberg-euler effective action: 75 years on, *International Journal of Modern Physics A* 27 (15) (2012) 1260004.
- [5] M. Soljačić, M. Segev, Self-trapping of electromagnetic beams in vacuum supported by qed nonlinear effects, *Phys. Rev. A* 62 (2000) 043817. doi:10.1103/PhysRevA.62.043817.
- [6] B. King, A. Di Piazza, C. H. Keitel, A matterless double slit, *Nat Photon* 4 (2) (2010) 92–94.
- [7] W. Heisenberg, H. Euler, Folgerungen aus der diracschen theorie des positrons, *Zeitschrift für Physik* 98 (11-12) (1936) 714–732.
- [8] Extreme light infrastructure, <http://www.eli-laser.eu/>.
- [9] The vulcan 10 petawatt project, <http://www.clf.stfc.ac.uk/CLF/Facilities/Vulcan/The+Vulcan+10+Petawatt+Project/14684.aspx>.
- [10] V. Yanovsky, V. Chvykov, G. Kalinchenko, P. Rousseau, T. Planckon, T. Matsuoka, A. Maksimchuk, J. Nees, G. Cheriaux, G. Mourou, K. Krushelnick, Ultra-high intensity- 300-tw laser at 0.1 hz repetition rate., *Opt. Express* 16 (3) (2008) 2109–2114.
- [11] T. Heinzl, A. Ilderton, Exploring high-intensity qed at eli, *The European Physical Journal D* 55 (2) (2009) 359–364.
- [12] HIBEF, <http://www.hzdr.de/db/Cms?pNid=427&pOid=35325>.
- [13] M. Vranic, G. T., R. A. Fonseca, L. O. Silva, Quantum radiation reaction in head-on laser-electron beam interaction, *ArXiv* 1511.04406.
- [14] D. Green, C. Harvey, Simla: Simulating particle dynamics in intense laser and other electromagnetic fields via classical and quantum electrodynamics, *Computer Physics Communications* 192 (2015) 313 – 321. doi:<http://dx.doi.org/10.1016/j.cpc.2015.02.030>.
- [15] T. G. Blackburn, C. P. Ridgers, J. G. Kirk, A. R. Bell, Quantum radiation reaction in laser-electron-beam collisions, *Phys. Rev. Lett.* 112 (2014) 015001. doi:10.1103/PhysRevLett.112.015001.
- [16] N. V. Elkina, A. M. Fedotov, I. Y. Kostyukov, M. V. Legkov, N. B. Narozhny, E. N. Nerush, H. Ruhl, Qed cascades induced by circularly polarized laser fields, *Phys. Rev. ST Accel. Beams* 14 (2011) 054401.
- [17] M. Vranic, T. Grismayer, J. Martins, R. Fonseca, L. Silva, Particle merging algorithm for pic codes, *Computer Physics Communications* 191 (2015) 65 – 73. doi:<http://dx.doi.org/10.1016/j.cpc.2015.01.020>.
- [18] T. Grismayer, M. Vranic, J. L. Martins, R. Fonseca, S. L. O., Seeded qed cascades in counter propagating laser pulses, *ArXiv* 1511.07503, submitted to *Physical Review E*.
- [19] T. Grismayer, M. Vranic, J. L. Martins, R. A. Fonseca, L. O. Silva, Laser absorption via quantum electrodynamics cascades in counter propagating laser pulses, *Physics of Plasmas* 23 (5). doi:<http://dx.doi.org/10.1063/1.4950841>.
- [20] C. P. Ridgers, C. S. Brady, R. Ducloux, J. G. Kirk, K. Bennett, T. D. Arber, A. R. Bell, Dense electron-positron plasmas and bursts of gamma-rays from laser-generated quantum electrodynamic plasmas, *Physics of Plasmas* 20 (5). doi:<http://dx.doi.org/10.1063/1.4801513>.
- [21] M. Vranic, J. L. Martins, J. Vieira, R. A. Fonseca, L. O. Silva, All-optical radiation reaction at 10^{21} W/cm², *Phys. Rev. Lett.* 113 (2014) 134801. doi:10.1103/PhysRevLett.113.134801.
- [22] A. Gonoskov, S. Bastrakov, E. Efimenko, A. Ilderton, M. Marklund, I. Meyerov, A. Muraviev, A. Sergeev, I. Surmin, E. Wallin, Extended particle-in-cell schemes for physics in ultrastrong laser fields: Review and developments, *Phys. Rev. E* 92 (2015) 023305. doi:10.1103/PhysRevE.92.023305.
- [23] J. Pétri, A 3+ 1 formalism for quantum electrodynamical corrections to maxwell equations in general relativity, *Monthly Notices of the Royal Astronomical Society* 451 (4) (2015) 3581–3586.
- [24] R. A. Fonseca, L. O. Silva, F. S. Tsung, V. K. Decyk, W. Lu, C. Ren, W. B. Mori, S. Deng, S. Lee, T. Katsouleas, J. C. Adam, OSIRIS: A three-dimensional, fully relativistic particle in cell code for modeling plasma based accelerators, Vol. 2331, Springer Berlin / Heidelberg, 2002.
- [25] K. Yee, Numerical solution of initial boundary value problems

- involving maxwell's equations in isotropic media, *Antennas and Propagation, IEEE Transactions on* 14 (3) (1966) 302–307.
- [26] Allen.Taflove, S. C. Hagness, *Computational Electrodynamics*, Artech House; 3 edition (May 31, 2005), 2005.
 - [27] J. McKenna, P. M. Platzman, Nonlinear interaction of light in a vacuum, *Phys. Rev.* 129 (1963) 2354–2360. doi:10.1103/PhysRev.129.2354.
 - [28] R. Baier, P. Breitenlohner, The vacuum refraction index in the presence of external fields, *Il Nuovo Cimento B* (1971-1996) 47 (1) (2015) 117–120. doi:10.1007/BF02712312.
 - [29] E. Brezin, C. Itzykson, Polarization phenomena in vacuum nonlinear electrodynamics, *Phys. Rev. D* 3 (1971) 618–621. doi:10.1103/PhysRevD.3.618.
 - [30] B. King, P. Böhl, H. Ruhl, Interaction of photons traversing a slowly varying electromagnetic background, *Phys. Rev. D* 90 (2014) 065018. doi:10.1103/PhysRevD.90.065018.
 - [31] N. Narozhny, A. Fedotov, Third-harmonic generation in a vacuum at the focus of a high-intensity laser beam, *Laser Physics* 17 (4) (2007) 350–357. doi:10.1134/S1054660X0704010X.
 - [32] A. Di Piazza, K. Z. Hatsagortsyan, C. H. Keitel, Harmonic generation from laser-driven vacuum, *Phys. Rev. D* 72 (2005) 085005. doi:10.1103/PhysRevD.72.085005.
 - [33] G. Zavattini, U. Gastaldi, R. Pengo, G. Ruoso, F. D. Valle, E. Milotti, Measuring the magnetic birefringence of vacuum: The pvlas experiment, *International Journal of Modern Physics A* 27 (15) (2012) 1260017.
 - [34] J. Jackson, *Classical Electrodynamics*, Wiley; 3 edition, 1998.
 - [35] A. Di Piazza, K. Z. Hatsagortsyan, C. H. Keitel, Light diffraction by a strong standing electromagnetic wave, *Phys. Rev. Lett.* 97 (2006) 083603.
 - [36] V. Dinu, T. Heinzl, A. Ilderton, M. Marklund, G. Torgrimsson, Photon polarization in light-by-light scattering: Finite size effects, *Phys. Rev. D* 90 (2014) 045025.